International Journal of Heat and Fluid Flow 31 (2010) 776–784

Contents lists available at ScienceDirect

International Journal of Heat and Fluid Flow

journal homepage: www.elsevier.com/locate/ijhff

Experimental study on turbulent mixing process in cross-flow type T-junction

Masafumi Hirota [a,*], Eri Mohri [b], Hideo Asano [c], Hiroki Goto [d]

[a] Department of Mechanical Engineering, Mie University, Kurimamachiya-cho 1577, Tsu-city 514-850, Japan
[b] Department of Mechanical Engineering, Nagoya University, Furo-cho, Chikusa-ku, Nagoya 464-8603, Japan
[c] Air-Conditioning Testing & Evaluation Department, DENSO Corporation, Showa-cho, Kariya 448-8661, Japan
[d] Nagoya Aerospace Systems Works, Mitsubishi Heavy Industry, Oye-cho, Minato-ku, Nagoya 455-8515, Japan

ARTICLE INFO

Article history:
Received 16 December 2009
Received in revised form 30 March 2010
Accepted 15 April 2010
Available online 18 May 2010

Keywords:
Turbulent mixing
T-junction
PIV
Turbulent heat flux
Flow visualization
POD

ABSTRACT

This study was conducted to clarify how two fluids with different temperature are mixed turbulently in a cross-flow type T-junction. The characteristics of the velocity and temperature fields in the channel were investigated experimentally, and the flow visualization was conducted to make clear the detailed behavior of the interface between two flows in the flow-merging region. We extracted the dominant structures of the velocity and concentration fields by proper orthogonal decomposition (POD). It is clarified that the interface of two flows is oscillating vertically and several discrete longitudinal eddies are superposed on it. We have concluded that the vertical oscillation of the interface is caused by the fluctuation of the streamwise velocity component, and the mushroom-like eddies are caused by the vertical fluctuating velocity; the former produces the turbulent heat flux in the streamwise direction, and the latter produces that in the vertical direction.

1. Introduction

A cross-flow type T-junction in which two flows with different velocities, temperatures, and/or concentrations are mixed turbulently is encountered in various thermal equipment, e.g., chemical reactor, combustion chamber, piping system in power plants. One of the typical mixing T-junctions is found in the HVAC (Heating, Ventilating, Air-conditioning) unit that is used for an automobile air-conditioning system (Kitada et al., 2000). Fig. 1 shows a schematic diagram of an automobile HVAC unit. It contains a fan, an evaporator and a heater-core in a plastic case. Air taken by the fan is once cooled to 5 °C by the evaporator to reduce humidity, and a part of this cold air is heated to about 80 °C by the heater-core. Since these temperatures of hot and cold airflows are fixed in the automobile A/C system, the temperature of air blown into the cabin is controlled by mixing them in the HVAC unit. The temperature distribution of the mixed airflow requested in the cabin is realized by controlling the flow-rate ratio of two flows, which is determined by the opening of the air-mix door located between the evaporator and the heater-core. In the bi-level mode shown in Fig. 1, the hot and cold airflows impinge at nearly right angles, and this situation can be modeled by the turbulent thermal mixing of hot and cold airflows in the cross-flow type T-junction with rectangular cross sections as shown in Fig. 2.

The flow field in the mixing T-junction is accompanied by the flow separation and reattachment, secondary flow, and strong turbulence. Therefore, it is expected that the turbulent heat transport process between the hot and cold airflows is quite complex. Moreover, the downsizing of the HVAC unit is an important subject in the development of the automobile A/C system, and the promotion and control of the mixing of hot and cold airflows are key issues to achieve it. In order to develop effective methods of the mixing promotion and control, one has to fully understand the detailed flow characteristics and mechanism of the thermal mixing of two flows in the T-junction. In the studies on mixing T-junctions conducted to date, the flow structure resulting from the interaction between the main flow and the branch flow has been examined in detail (Kelso et al., 1996; Haven and Kurosaka, 1997; Bruecker, 1997; Wu et al., 2003). Moreover, the characteristics of the temperature field have been investigated as well. In particular, the temperature fluctuation near the channel wall has been examined to make clear the mechanism of the thermal striping phenomena that occur in a nuclear power plant (Kawamura et al., 2002; Igarashi et al., 2002; Fukushima et al., 2003; Yuki et al., 2004; Nakajima et al., 2005; Tanaka et al., 2005). In the application to the automobile HVAC unit, the heat transfer between the hot airflow and cold one is important, but few data are available on the detailed mechanism of heat transfer between two flows in a T-junction (Kok and van der Wal, 1996).

With these points as background, the authors have been conducting experimental study on turbulent mixing of hot and cold

* Corresponding author. Tel./fax: +81 59 231 9385.
E-mail address: hirota@mach.mie-u.ac.jp (M. Hirota).

0142-727X/$ - see front matter © 2010 Elsevier Inc. All rights reserved.
doi:10.1016/j.ijheatfluidflow.2010.04.006

Nomenclature

A	half-width of the channel
B	height of the branch channel = $H/2$
C	time-averaged local concentration
c	fluctuating concentration
H	height of the main channel cross section
T	time-averaged local temperature of the mixed flow
ΔT	initial temperature difference between the hot and cold flows
t	fluctuating temperature
U, V, W	time-averaged velocity components in the X-, Y- and Z-directions
U_0	mean velocity in the main channel before the mixing
u, v, w	fluctuating velocity components in the X-, Y- and Z-directions
u', v', w'	root-mean-square of u, v and w
X, Y, Z	coordinate system (see Fig. 2)
$\boldsymbol{\Phi}$	eigenfunction of POD

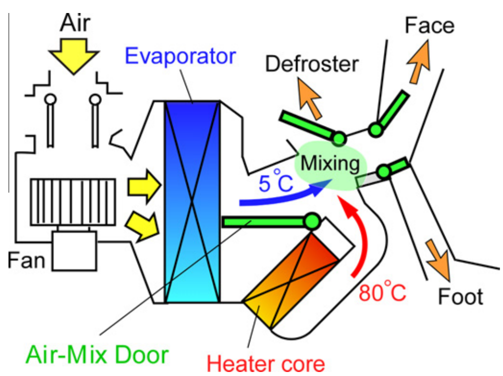

Fig. 1. HVAC unit for automobiles.

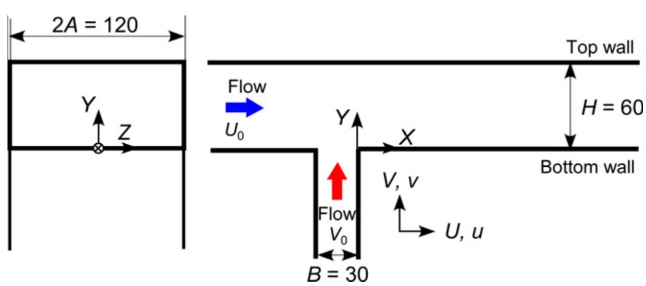

Fig. 2. Schematic diagram of the test channel.

airflows in a T-junction with rectangular cross sections and have made clear the characteristics of the velocity and temperature fields after the merging of two flows (Hirota et al., 2005, 2006). The present study has been conducted to clarify experimentally the detailed mechanism of turbulent heat transfer between hot and cold flows that are mixed in a T-junction. After overviewing the characteristics of velocity and temperature fields in the channel, the instantaneous structure of the mixing interface between two flows is examined based on the results of the flow visualization. The dominant structures of the fluctuating velocity and concentration (temperature) fields in the mixing layer are investigated by analyzing the results of PIV and flow visualization with the proper orthogonal decomposition (POD) (Hilberg et al., 1994; Graftieaux et al., 2001). The detailed mechanism of turbulent heat transport process between the hot and cold airflows mixed in the T-junction is discussed synthetically based on these analyses of the velocity and concentration fields.

2. Experimental apparatus and method

Fig. 2 shows a schematic diagram of the test channel and the coordinate system. The horizontal channel is the main channel, and the branch channel is joined to it at right angles to form a T-junction. The airflows in both channels are mixed in the T-junction after flowing through the heat exchangers, settling chambers and contraction flow nozzles. The height of the main channel H is 60 mm and the width $2A$ is 120 mm. The height (X-way length) of the branch cross section B is 30 mm and the width of the branch is 120 mm. In most studies on the mixing T-junction conducted to date, the diameter or width of the branch has been smaller than that of the main channel. In the present study, the width of the branch is the same as that of the main channel, and this is a geometric feature of the HVAC unit. It is thought that this difference of the channel geometry exerts considerable influences upon the flow structure and resulting temperature field after the flow merging. The origin of the coordinate system is at the spanwise centerline of the downstream edge of the T-junction. In a real HVAC unit, the exit of the mixing zone corresponds to the location of X/B = 2–3. The mean and fluctuating velocity components are denoted as U, V, W, and u, v, w, respectively.

We made experiments keeping the Reynolds number of the main-channel flow before the mixing (=$U_0 d_h/\nu$, where d_h denotes the hydraulic diameter of the main channel) at 1.5×10^4. The bulk velocity of the branch flow was set at the same value as that of the main flow U_0. The velocity distributions were measured by a 2-D PIV system (TSI Inc.) under an isothermal condition. For a statistical analysis, the mean velocity and turbulence intensities were computed by an ensemble average of 500 instantaneous velocity fields. The time-averaged local temperature distributions were measured by a thermocouple rake. Moreover, the simultaneous measurements of the fluctuating velocity and temperature were conducted by combining LDV (TSI Inc., Model 9000) and the cold-wire thermometer (Tsukasa Sokken, HG-037A) (Hirota et al., 2004) to make clear the distributions of turbulent heat fluxes, which dominate the heat transfer between the hot and cold airflows. In these measurements of the temperature field, the bulk temperature of the main-channel flow T_c and that of the branch flow T_h were set at 12 °C and 60 °C, respectively. Fig. 3a shows the distributions of the mean velocity U and RMS of the fluctuating velocity component u', and Fig. 3b shows the mean temperature T; they were measured in the symmetric plane of the channel (Z/A = 0) at X/B = −3. Both the mean velocity and mean temperature show uniform distributions over the region covering about 80% of channel height H. The turbulence intensities in the core regions are about 4% of the bulk velocities.

Then the flow visualization was conducted in the flow-merging region to make clear the detailed behavior of the interface between the main and branch flows. Particles of dioctyl sebacate generated by a Laskin nozzle (Kaehler et al., 2002) were suspended in the branch flow, and the mixing interface between two flows visualized by a laser-light sheet was captured by the digital high-speed video camera (Kodak, Motioncorder) as time-resolved images. The typical frame rate was 250 frames/s. The captured images were converted to the concentration distributions with a calibration of

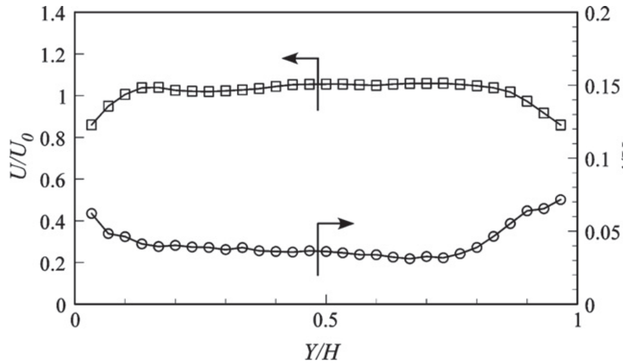

(a) Mean velocity U/U_0 and turbulence intensity u'/U_0

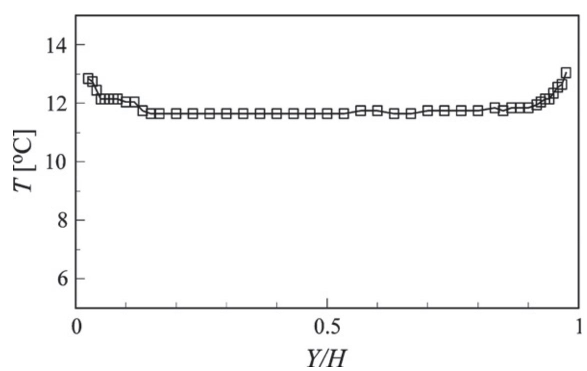

(b) Mean temperature T

Fig. 3. Inlet conditions before the T-junction (main channel, $X/B = -3$). (a) Mean velocity U/U_0 and turbulence intensity u'/U_0. (b) Mean temperature T.

the intensity distribution in the laser sheet. As shown later, these concentration distributions are analogous to the temperature distributions in the mixing layer. The dominant structures of the velocity and concentration fields were extracted by applying POD to the results obtained by PIV and the flow visualization.

3. Results and discussion

3.1. Overview of velocity and temperature fields

3.1.1. Velocity field

In this section, we describe the global characteristics of the velocity field measured by PIV. Although the flow field has a three-dimensional structure, the results obtained in the symmetric plane of the channel ($Z/A = 0$) are mainly addressed here for brevity. More detailed characteristics of the flow field are described in the literature (Hirota et al., 2005).

Fig. 4 shows the mean velocity vector diagram. The time-averaged interface between the main and branch flows is shown by a

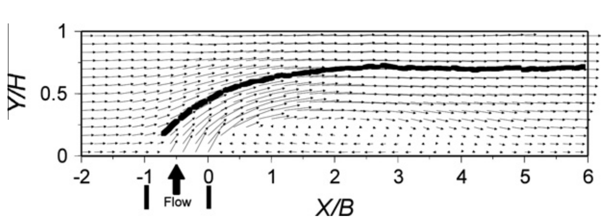

Fig. 4. Mean velocity vector diagram in the symmetric plane of $Z/A = 0$. (The solid lines show the time-averaged interface between the main and branch flows obtained by the flow visualization.)

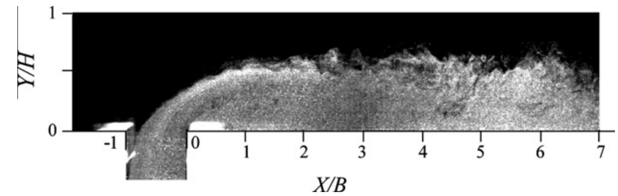

Fig. 5. Visualized image of the interface between two flows in $Z/A = 0$. (The solid lines show the time-averaged interface between the main and branch flows obtained by the flow visualization.)

solid line, which was obtained by the flow visualization. Fig. 5 is an example of snapshots of the instantaneous interface of two flows. The branch flow was seeded by oil mist and the images visualized by a laser sheet were captured by a digital video camera. They were converted to binary format images, and the time-averaged interface between two flows was obtained as an ensemble average of 100 snapshots of the instantaneous interface. In Fig. 4, the upward velocity component is relatively large in the flow-merging region ($-1 < X/B < 0$), but downward flows are observed in the further downstream region of $X/B > 3$. The flow that enters the main channel from the branch is separated at the downstream edge of the T-junction ($X/B = 0$), and a large separation bubble is formed along the bottom wall of the channel.

Next, the distributions of root-mean-square of the fluctuating velocity components in the streamwise direction u'/U_0 and the vertical directions v'/U_0 are shown in Fig. 6a and b, respectively. The time-averaged interface between the main and branch flows is shown by a red line. Fig. 7 shows the close-ups of u'/U_0 and v'/U_0 in the flow-merging region of $-1 < X/B < 0$, and the upper and lower boundaries of the thermal mixing layer are shown by blue lines. These boundaries of the thermal mixing layer were defined as locations at which the mean temperature gradient $\partial T/\partial Y$ becomes zero. In the flow-merging region, u' attains the maximum near the upper boundary of the mixing layer. In the downstream region of $X/B > 0$, u' increases remarkably in the shear layer around the reverse flow region. The distribution of v' is qualitatively similar to that of u', but v' shows the local maximum around the center of the mixing layer in the flow-merging region. In the region of

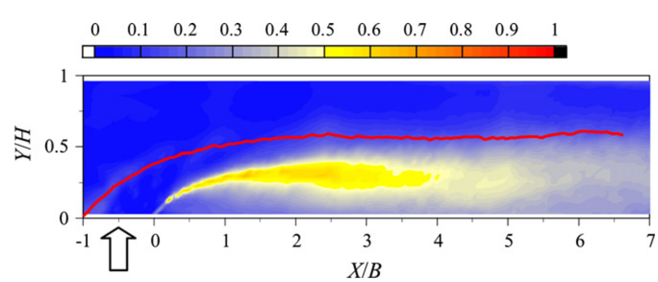

(a) u'/U_0

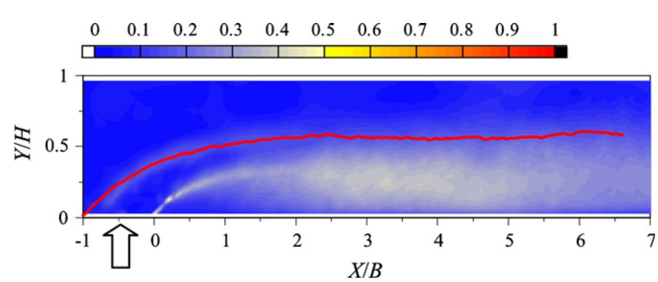

(b) v'/U_0

Fig. 6. Contour maps of turbulence intensities in $Z/A = 0$.

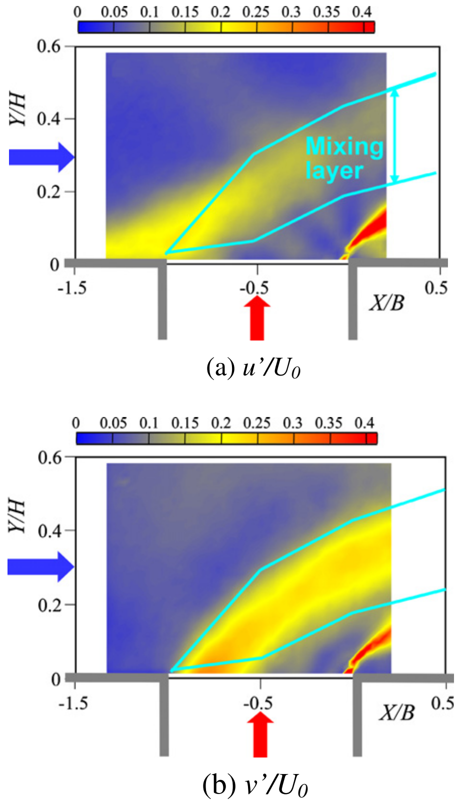

Fig. 7. Close-ups of turbulence intensities in the flow-merging region. (The solid lines show the upper and lower boundaries of the thermal mixing layer.)

$X/B > 2$, however, v' attains the maximum in the shear layer around the reverse flow region.

3.1.2. Mean temperature distribution

The distributions of the time-averaged local temperature $(T - T_c)/\Delta T$ obtained in the symmetric plane of the channel $Z/A = 0$ are shown in Fig. 8. The red lines in the figure correspond to the upper and lower boundaries of the thermal mixing layer, and the green line shows the location at which $-\partial T/\partial Y$ attains the maximum. The broken line near the bottom wall shows the boundary of the reverse flow region. For the sake of visibility, the scale in the X-direction is magnified by a factor of two in comparison with that in the Y-direction. Just after the flow merging, the thickness of the thermal mixing layer amounts to 25–30% of the channel height, suggesting that the hot and cold flows are mixed quite quickly by their impingement. Then the thermal mixing layer develops downward gradually as the flow proceeds downstream until its lower boundary overlaps with the reverse flow region. On the other hand, the upward development of the mixing layer is stagnant in comparison with the downward development.

3.1.3. Turbulent heat fluxes

Next, the distributions of the turbulent heat fluxes $\overline{ut}$ and $\overline{vt}$ are presented. Fig. 9 shows the component in the Y-direction $\overline{vt}$, which is thought to dominate the turbulent heat transport between the hot and cold flows in the mixing layer. It attains the local maximum near the center of the thermal mixing layer and decreases to zero around the upper and lower edges of the thermal mixing layer. A detailed observation of this figure reveals that the value of this local maximum of $\overline{vt}$ is the largest in the flow-merging region and decreases gradually in the streamwise direction.

The streamwise component of the turbulent heat flux $\overline{ut}$ is presented in Fig. 10. In the flow-merging region, $\overline{ut}$ shows the maximum near the center of the thermal mixing layer. As observed in the figure, the upper and lower boundaries of the thermal mixing layer are inclined with respect to the X-axis in this region, thus the mean temperature gradient $\partial T/\partial X$ is in the same level as $\partial T/\partial Y$. This means that $\overline{ut}$ as well as $\overline{vt}$ contributes to the turbulent heat transport between the hot and cold flows in this region. It is thought that these contributions of both $\overline{ut}$ and $\overline{vt}$ in the flow-merging region bring about such a quick mixing of hot and cold flows there as described above. After the flow-merging region, $\overline{ut}$ shows large values while $\partial T/\partial X$ is quite small. Therefore, $\overline{ut}$ presents no more than a passing of heat in the streamwise direction there and does not contribute substantially to the turbulent heat transfer between two flows. In this paper, attention is directed to the mechanism of heat transfer between the hot and cold flows in the flow-merging region, in which two flows are mixed quite quickly.

3.2. Visualization of interface between main and branch flows

In order to make clear the detailed structure of the mixing interface between the main and branch flows in the flow-merging region, we made the flow visualization. Oil particles were seeded to the branch flow, and the interface of two flows visualized by a laser-light sheet was captured by the digital high-speed video camera at a rate of 250 frames/s to make clear its time-series behavior.

Fig. 11a shows an example of the snapshots captured in the symmetric plane of the channel $Z/A = 0$. From the time-series images, it was observed that the reversal of the branch flow to the upstream side of the main channel and the inflow of the main flow to the branch occurred alternately in time at the first (upstream side) edge of the T-junction. The interface of two flows

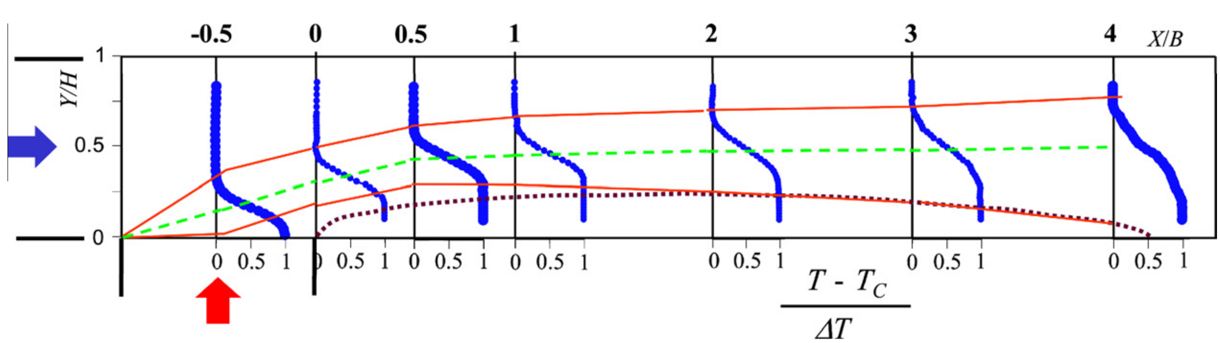

Fig. 8. Mean temperature distributions in $Z/A = 0$. (The red lines show the upper and lower boundaries of the thermal mixing layer, and the green line shows the location of the maximum $-\partial T/\partial Y$. The broken line shows the boundary of the reverse flow region.) (For interpretation of the references to colour in this figure legend, the reader is referred to the web version of this article.)

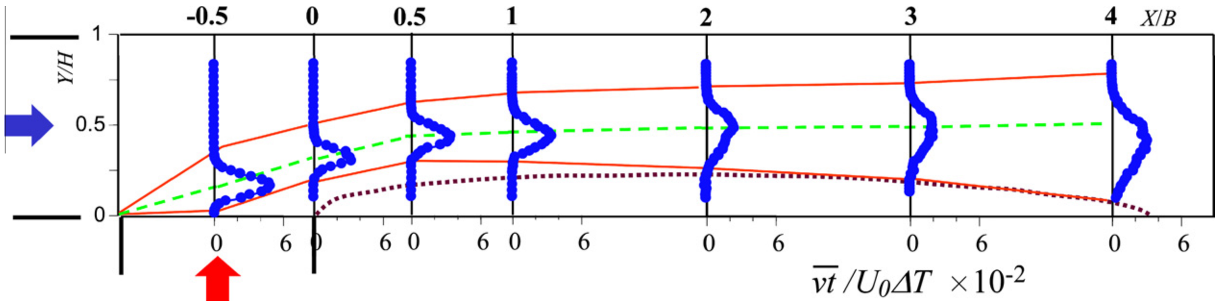

Fig. 9. Turbulent heat flux in the vertical direction $\overline{vt}$. (The red lines show the upper and lower boundaries of the thermal mixing layer, and the green line shows the location of the maximum $-\partial T/\partial Y$. The broken line shows the boundary of the reverse flow region.) (For interpretation of the references to colour in this figure legend, the reader is referred to the web version of this article.)

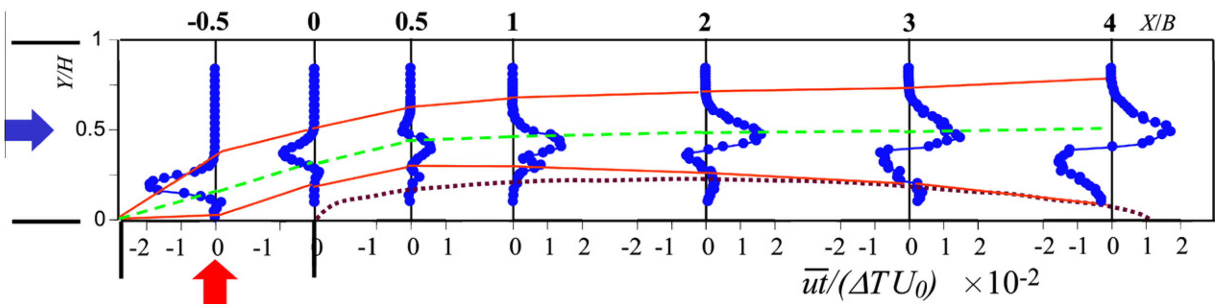

Fig. 10. Turbulent heat flux in the streamwise direction $\overline{ut}$. (The red lines show the upper and lower boundaries of the thermal mixing layer, and the green line shows the location of the maximum $-\partial T/\partial Y$. The broken line shows the boundary of the reverse flow region.) (For interpretation of the references to colour in this figure legend, the reader is referred to the web version of this article.)

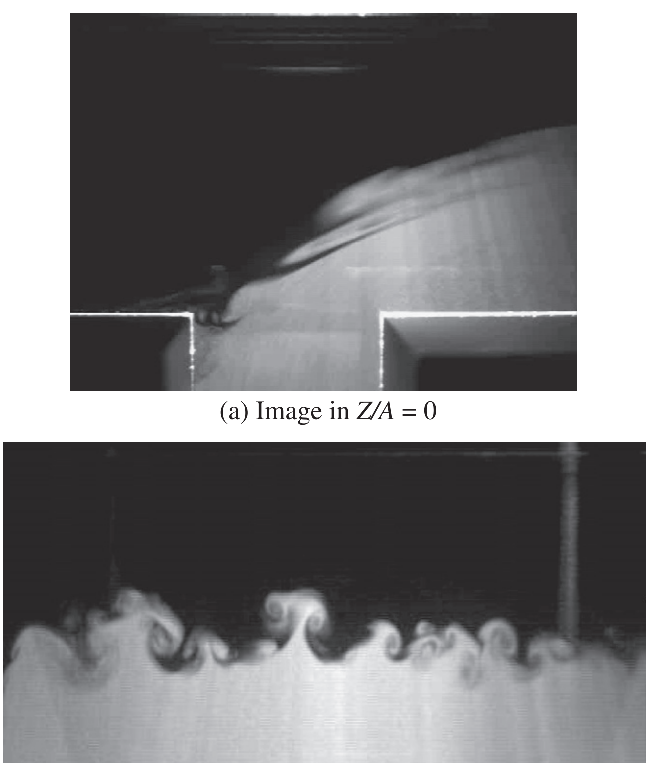

(a) Image in $Z/A = 0$

(b) Image in $X/B = 0$

Fig. 11. Visualized interface of two flows.

was deformed quite irregularly and orderly eddies such as those generated by the Kelvin–Helmholtz instability were not observed.

The snapshot obtained in the cross section at $X/B = 0$ is shown in Fig. 11b. Mushroom-like discrete longitudinal eddies (Hu et al., 2000) are clearly observed along the interface of two flows. Moreover, from the observation of the time-series images, we found that the whole interface of two flows was oscillating periodically in the Y-direction (vertically). These results show that the interface of the main and branch flows has complex three-dimensional unsteady characteristics.

In this study, the results of the flow visualization were converted to the concentration distributions by compensating the uneven distribution of the light intensity in the laser sheet. Fig. 12 shows a comparison of distributions of the mean temperature $(T - T_c)/\Delta T$ and mean concentration C/C_0 measured in $Z/A = 0$, where C_0 denotes the mean concentration of the branch flow. The mean concentration distribution was calculated by an ensemble average of 1200 instantaneous concentration fields. It is confirmed that the distributions of the mean concentration in the mixing layer agree closely with those of the mean temperature, although the concentration mixing layer is shifted upward in comparison with the thermal mixing layer. This difference is caused by

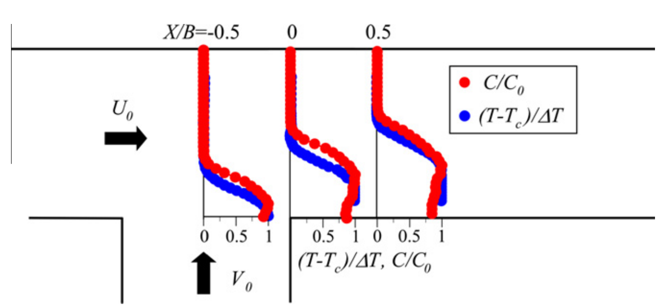

Fig. 12. Comparison of mean temperature and mean concentration distributions.

the centrifugal force exerted on oil particles in the branch flow. We applied the proper orthogonal decomposition (POD) to the fluctuating velocity and concentration fields in the flow-merging region to extract dominant structures that contribute to the heat transfer between the hot and cold airflows.

3.3. Proper orthogonal decomposition

In this study, we applied POD analyses to the fluctuating velocity components u and v measured by PIV and to the fluctuating concentration c obtained by the flow visualization in the flow-merging region. Here we briefly explain the outline of the direct POD used in this study (Hilberg et al., 1994; Graftieaux et al., 2001).

In PIV or flow visualization, instantaneous velocity or concentration can be measured at M points in space and N points in time, i.e., a set of N snapshots. We define $f(\boldsymbol{x}, t)$ as a fluctuating velocity or concentration in a finite spatial domain S, and $f(\boldsymbol{x}, t)$ can be expanded into a finite series of M orthogonal eigenfunctions $\boldsymbol{\Phi}^{(k)}(\boldsymbol{x})$ with time coefficients $a^{(k)}(t)$ as follows.

$$f(\boldsymbol{x},t) = \sum_{k=1}^{M} a^{(k)}(t)\boldsymbol{\Phi}^{(k)}(\boldsymbol{x}) \tag{1}$$

$$a^{(k)}(t) = \int f(\boldsymbol{x},t)\boldsymbol{\Phi}^{(k)}(\boldsymbol{x})d\boldsymbol{x} \tag{2}$$

The eigenfunction $\boldsymbol{\Phi}^{(k)}(\boldsymbol{x})$, which represents the spatial structure of the fluctuating velocity or concentration field, is obtained as a solution of the following equation.

$$\int_S R(\boldsymbol{x},\boldsymbol{x}')\boldsymbol{\Phi}^{(k)}(\boldsymbol{x}')d\boldsymbol{x}' = \lambda^{(k)}\boldsymbol{\Phi}^{(k)}(\boldsymbol{x}) \tag{3}$$

$$R(\boldsymbol{x},\boldsymbol{x}') = \frac{1}{N}\sum_{i=1}^{N} f(\boldsymbol{x},t_i)f(\boldsymbol{x}',t_i) \tag{4}$$

$R(\boldsymbol{x}, \boldsymbol{x}')$ is the two-point spatial correlation matrix, and $\lambda^{(k)}$ is the eigenvalue of the kth mode that is ordered in a decreasing order as $\lambda^{(1)} > \lambda^{(2)} > \lambda^{(3)} > \cdots$. The superscript k denotes the eigenmode ($k = 1, 2, 3, \ldots, M$). The total "energy" of $f(\boldsymbol{x}, t)$, which is denoted as E and defined below, is expressed as a sum of all the eigenvalues.

$$E = \int_S \langle f^2(\boldsymbol{x},t)\rangle d\boldsymbol{x} = \sum_{k=1}^{M}\lambda^{(k)} \tag{5}$$

The bracket $\langle\cdot\rangle$ in Eq. (5) denotes an ensemble average. The contribution ratio made by the kth mode to the total energy E_k is given by the following equation.

$$E_k = \lambda^{(k)} / \sum_{k=1}^{M}\lambda^{(k)} \tag{6}$$

From these definitions of the eigenmode and eigenvalue, it follows that the structure expressed by the lower mode has a larger contribution to the total energy. This means that a dominant structure of the fluctuating velocity or concentration field can be reconstructed by several lower modes extracted by the POD analysis. In the following, we show the results of the analyses that are applied to the fluctuating velocity and concentration fields measured in the flow-merging region, and discuss the mechanism of turbulent heat transport between the hot and cold flows in the T-junction.

3.4. Results of POD

3.4.1. Fluctuating concentration field in a cross section

At first, the results of POD analysis applied to the fluctuating concentration c measured in the cross section of $X/B = 0$ are presented; this cross section includes the second edge (downstream edge) of the T-junction. Fig. 13a shows the eigenfunction of the first mode $\boldsymbol{\Phi}_c^{(1)}\boldsymbol{x}$, which represents the most dominant spatial structure of the fluctuating concentration field. The region of negative sign is distributed almost uniformly in the spanwise direction. This distribution of $\boldsymbol{\Phi}_c^{(1)}\boldsymbol{x}$ corresponds to the vertical oscillation of the mixing interface of two flows found by the observation of time-series images of the visualized flow as described in Section 3.2. This means that the mixing interface is oscillating in the Y-direction keeping a uniform structure in the Z-direction.

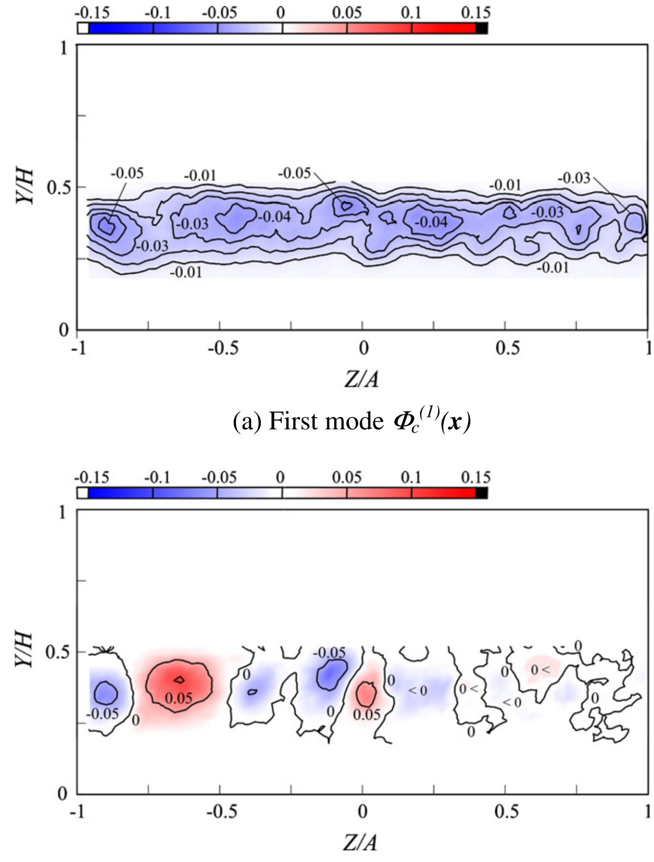

Fig. 13. Eigenfunctions for the fluctuating concentration c in $X/B = 0$.

In the eigenfunction of the second mode $\boldsymbol{\Phi}_c^{(2)}\boldsymbol{x}$ shown in Fig. 13b, the regions of positive and negative values are distributed alternately in the spanwise direction. This $\boldsymbol{\Phi}_c^{(2)}\boldsymbol{x}$ corresponds to the mushroom-like longitudinal eddies observed in Fig. 11b. These results of the POD applied to the fluctuating concentration field mean that the interface of two flows in the flow-merging region is oscillating vertically keeping a uniform structure in the spanwise direction, and discrete longitudinal eddies are superposed upon this oscillating interface. This enforces our observational results of the time-series images of the mixing interface at $X/B = 0$.

3.4.2. Fluctuating velocity field in a cross section

Next, in order to make clear the mechanism that causes such a complex behavior of the mixing interface of two flows described above, we applied the POD to the fluctuating velocity component in the Y-direction v measured by PIV in the cross section of $X/B = 0$. Fig. 14a and b shows the eigenfunctions of the first mode $\boldsymbol{\Phi}_v^{(1)}\boldsymbol{x}$ and of the second mode $\boldsymbol{\Phi}_v^{(2)}\boldsymbol{x}$, respectively. In both eigenfunctions, the region of positive and negative values are distributed alternately in the spanwise direction, and these results are qualitatively similar to $\boldsymbol{\Phi}_c^{(2)}\boldsymbol{x}$ shown in Fig. 13b. Therefore, it is thought that the flow expressed by $\boldsymbol{\Phi}_v^{(1)}\boldsymbol{x}$ and $\boldsymbol{\Phi}_v^{(2)}\boldsymbol{x}$ causes the mushroom-like longitudinal eddies on the mixing interface of two flows.

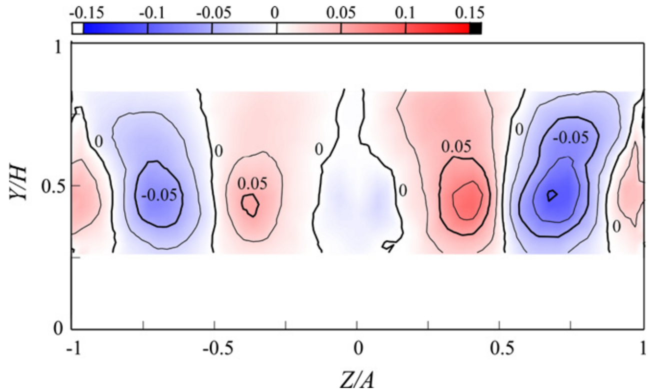

(a) First mode $\Phi_v^{(1)}(\boldsymbol{x})$

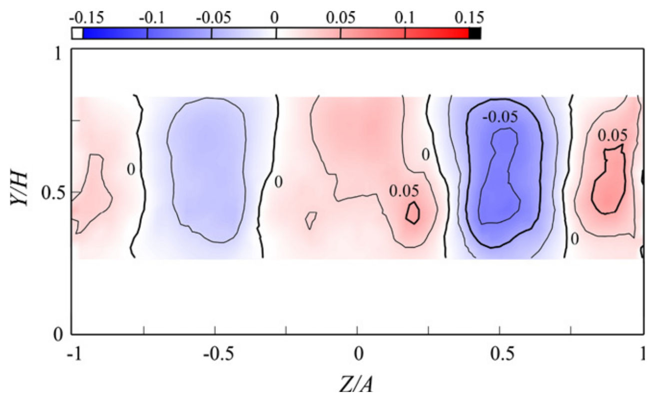

(b) Second mode $\Phi_v^{(2)}(\boldsymbol{x})$

Fig. 14. Eigenfunctions for the fluctuating velocity component v in $X/B = 0$.

In the POD analysis of v, however, the flow structure that was expected to cause the two-dimensional oscillation of the mixing interface in the Y-direction expressed by $\Phi_c^{(1)}\boldsymbol{x}$ was not extracted in higher modes. Hence, in order to clarify the flow structure that causes this oscillation, we applied POD to the streamwise fluctuating velocity component u measured in $Z/A = 0$ in the flow-merging region.

3.4.3. Fluctuating velocity field in a symmetric plane

Fig. 15 shows the result of the eigenfunction of the first mode $\Phi_u^{(1)}\boldsymbol{x}$. The blue line shows the upper boundary of the thermal mixing layer. It shows positive values over a large area around the mixing layer in the flow-merging region. This result means that the merging of two flows in the T-junction causes large-scale oscillation of the mixing interface in the X-direction. It is noticeable that

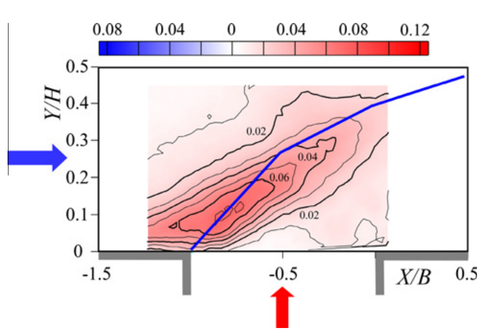

Fig. 15. Eigenfunction of the first mode for u ($\Phi_u^{(1)}\boldsymbol{x}$) in $Z/A = 0$.

$\Phi_u^{(1)}\boldsymbol{x}$ shows relatively large value in the region before the first edge of the T-junction. This suggests that the streamwise oscillation of the mixing interface is caused by the reversal of the branch flow to the main channel and the inflow of the main flow to the branch found at this edge by the flow visualization (described in Section 3.2).

From these results of POD for u and v, it follows that the oscillation of the mixing interface in the Y-direction suggested by $\Phi_c^{(1)}\boldsymbol{x}$ in Fig. 13a is caused not by v but by u. The mechanism of this vertical oscillation of the mixing interface caused by the streamwise fluctuating velocity component u is illustrated in Fig. 16. Since the interface of two flows in the flow-merging region is inclined with respect to the X-axis, this interface seems to move downward in $X/B = 0$ when u is positive, and vice versa. This idea is supported by the fact that the peak frequency of the concentration fluctuation reconstructed by the first mode of POD agreed well with that of u measured by the hot-wire anemometer in the flow-merging region. Fig. 17a shows the power spectrum of u measured by a hot-wire anemometer at $X/B = -0.5$ and $Y/H = 0.5$ in $Z/A = 0$. The ordinate has an arbitrary scale. The local peak frequency is found around 40 Hz. The power spectrum of concentration fluctuation reconstructed by the first mode of POD obtained in the cross section of $X/B = 0$ is shown in Fig. 17b. This result was obtained by FFT of the time coefficient $a^{(1)}(t)$ for $\Phi_c^{(1)}\boldsymbol{x}$ shown in Fig. 13a. The peak frequency in Fig. 17b agrees well with that observed in Fig. 17a. These results suggest that the vertical oscillation of the

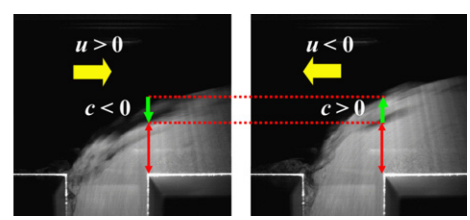

Fig. 16. Mechanism of vertical oscillation of the mixing interface by u. Left: $u > 0$, $c < 0$, right: $u < 0$, $c > 0$.

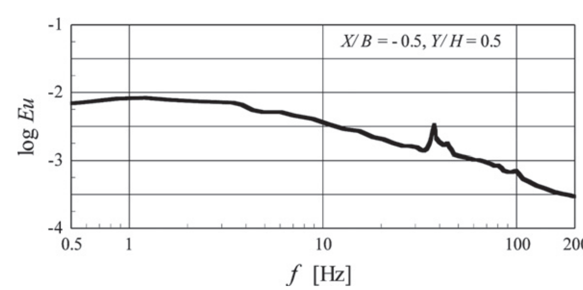

(a) Result of u measured at X/B = -0.5 and Y/H = 0.6 in Z/A = 0

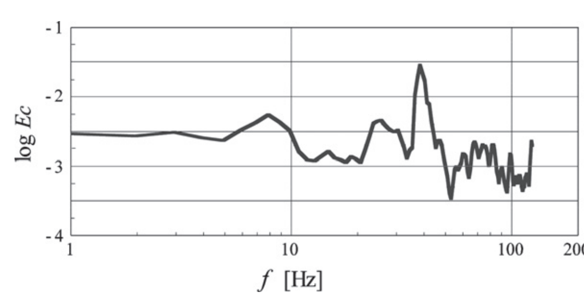

(b) Result of the time coefficient $a^{(1)}(t)$ for $\Phi_c^{(1)}(\boldsymbol{x})$ in $X/B = 0$

Fig. 17. Power spectra of fluctuating velocity and fluctuating concentration.

mixing interface observed in $X/B = 0$ is caused by the streamwise fluctuating velocity component u.

In conventional studies on turbulent mixing conducted to date, the scalar transport has been discussed in relation to the Kelvin–Helmholtz spanwise vortices generated along the interface between two flows (Hu et al., 2000; Pickett and Ghandhi, 2001, 2002). In the present study, however, the flow structure corresponding to those spanwise vortices is not extracted by POD in the flow-merging region, and $\overline{vt}$ is caused by the longitudinal eddies generated upon the oscillating interface of two flows. This mechanism of $\overline{vt}$ production is distinctive of the flow-merging region in this T-junction. As observed in Fig. 5, the structure corresponding to the Kelvin–Helmholtz spanwise vortices appears in the region of $X/B > 1$, and it is thought that these vortices would play an important role in turbulent heat transfer between the hot and cold flows in that region. Moreover, as described in Section 3.1.3., $\overline{ut}$ as well as $\overline{vt}$ contributes to the heat transfer between two flows in the flow-merging region, and $\overline{ut}$ is produced by the large-scale oscillation of the mixing interface in the X-direction. This mechanism of heat transfer in the streamwise direction would be also a unique feature of turbulent mixing in a flow-merging region of the T-junction. The contribution of the streamwise turbulent heat (mass) flux to the mixing of turbulent jet discharging into fluid was also pointed out by Law and Wang (2000). These results suggest that the turbulent mixing in the flow-merging region of the T-junction can be promoted efficiently by intensifying the streamwise oscillation of the main flow and/or increasing the generation of mushroom-like longitudinal eddies in the branch flow.

4. Conclusions

Experimental study has been conducted on turbulent thermal mixing of hot and cold airflows in a T-junction. The cross sections of the main channel and the branch are $120\,\text{mm} \times 60\,\text{mm}$ and $120\,\text{mm} \times 30\,\text{mm}$, respectively. The Reynolds number of the main-channel flow before the mixing is 1.5×10^4, and the bulk velocity of the branch flow is set at the same value as that of the main flow. The bulk temperature of the main-channel flow and that of the branch flow are set at 12 °C and 60 °C, respectively. The dominant structures of the velocity and concentration (temperature) fields in the flow-merging region have been extracted by POD, and the mechanism of turbulent heat transfer between two flows has been discussed synthetically based on these analyses of the velocity and concentration fields. The main conclusions are as follows.

(1) The flow that enters the main channel from the branch is separated at the downstream edge of the T-junction, and a large separation bubble is formed on the bottom wall. The turbulence intensities u' and v' show the local maximums in the mixing layer just after the merging of two flows, but they attain the maximums in the shear layer around the separation bubble in the further downstream region.

(2) Just after the flow merging, the thickness of the thermal mixing layer amounts to 25–30% of the channel height. This suggests that the hot and cold flows are mixed quite quickly by their impingement. Then the thermal mixing layer develops downward gradually as the flow proceeds downstream, but the upward development is stagnant in comparison with the downward development.

(3) In the flow-merging region of $-1 < X/B < 0$, the turbulent heat fluxes $\overline{ut}$ and $\overline{vt}$ attain the maximums near the center of the thermal mixing layer. Since the thermal mixing layer is inclined with respect to the X- and Y-axes in this region, both $\overline{ut}$ and $\overline{vt}$ contribute to the turbulent heat transfer between the hot and cold flows. These contributions of $\overline{ut}$ and $\overline{vt}$ bring about a quick thermal mixing of hot and cold flows in this region.

(4) The POD analyses applied to the fluctuating velocity and concentration fields in the cross section of $X/B = 0$ reveals that the interface of two flows in the flow-merging region is oscillating vertically keeping a uniform structure in the spanwise direction, and discrete mushroom-like discrete longitudinal eddies are superposed upon this oscillating interface. These longitudinal eddies are directly produced by the fluctuating velocity component v and contribute to the turbulent heat transport in the Y-direction.

(5) In the flow-merging region, a large-scale oscillation of the mixing interface in the X-direction occurs and it causes the vertical oscillation of the mixing interface observed in $X/B = 0$. This streamwise oscillation of the mixing interface is caused by the reversal of the branch flow to the upstream side of the main channel and the inflow of the main flow to the branch at the upstream edge of the T-junction, and contributes to the turbulent heat transport in the X-direction.

References

Bruecker, C., 1997. Study of the three-dimensional flow in a T-junction using a dual-scanning method for three-dimensional scanning-particle-image-velocimetry (3-D SPIV). Exp. Therm. Fluid Sci. 14, 35–44.
Fukushima, N., Fukagata, K., Kasagi, N., Noguchi, H., Tanimoto, K., 2003. Numerical and experimental study on turbulent thermal mixing in a T-junction flow. In: Proc. 6th ASME-JSME Joint Thermal Eng. Conf. TED-AJ03-582 (in CD-ROM).
Graftieaux, L., Michard, M., Grosjean, N., 2001. Combining PIV, POD and vortex identification algorithms for the study of unsteady turbulent swirling flows. Meas. Sci. Technol. 12, 1422–1429.
Haven, B.A., Kurosaka, M., 1997. Kidney and anti-kidney vortices in crossflow jets. J. Fluid Mech. 352, 27–64.
Hilberg, D., Lazik, W., Fiedler, H.E., 1994. The application of classical POD and snapshot POD in a turbulent shear layer with periodic structures. Appl. Sci. Res. 53, 283–290.
Hirota, M., Nakayama, H., Asano, H., Mizuno, Y., Hirayama, S., 2004. Simultaneous measurement of velocity and temperature in thermal mixing shear layer using LDV and cold wire. In: Proc. 12th Int. Symp. Appl. Laser Tech. Fluid Mech. (in CD-ROM).
Hirota, M., Asano, H., Nakayama, H., Asano, T., Hirayama, S., 2005. Three-dimensional structure of turbulent flow in mixing T-junction. JSME Int. J., Ser. B 49, 1070–1077.
Hirota, M., Asano, H., Nakayama, H., Asano, T., Goto, H., Hirayama, S., 2006. Turbulent thermal mixing of hot and cold airflows in T-junction. In: Proc. 13th Int. Heat Transfer Conf. TRB-11 (in CD-ROM).
Hu, H., Kobayashi, T., Saga, T., Segawa, S., Taniguchi, N., 2000. Particle image velocimetry and planar laser-induced fluorescence measurements on lobed jet mixing flows. Exp. Fluids (Suppl.), S.141–S.157.
Igarashi, M., Tanaka, M., Kawashima, S., Kamide, H., 2002. Experimental study on fluid mixing for evaluation of thermal striping in T-pipe junction. In: Proc. 10th Int. Conf. Nuclear Eng. ICONE10-22255.
Kaehler, C.J., Sammler, B., Kompenhans, J., 2002. Generation and control of tracer particles for optical flow investigation in air. Exp. Fluids 33, 736–742.
Kawamura, T., Shiina, K., Ohtsuka, M., Tanaka, I., Hirayama, H., Tanimoto, K., Fukuda, T., Sakashita, A., Mizutani, J., Minami, Y., Moriya, S., Madarame, H., 2002. Experimental study on thermal striping in a mixing tee with hot and cold water. In: Proc. 10th Int. Conf. Nuclear Eng. ICONE10-22214.
Kelso, R.M., Lim, T.T., Perry, A.E., 1996. An experimental study of round jets in cross-flow. J. Fluids Mech. 306, 111–144.
Kitada, M., Asano, H., Kanbara, H., Akaike, S., 2000. Development of automotive air-conditioning system basic performance simulator: CFD technique development. JSAE Rev. 21, 91–96.
Kok, J.B.W., van der Wal, S., 1996. Mixing in T-junctions. Appl. Math. Modell. 20, 232–243.
Law, A.W-K., Wang, H., 2000. Measurement of mixing processes with combined digital particle image velocimetry and planar laser induced fluorescence. Exp. Therm. Fluid Sci. 22, 213–229.
Nakajima, N., Hibara, H., Muramatsu, T., Tanaka, M., Iwamoto, Y., Ochi, J., 2005. Effects of turbulence promoter on flow in T-junction piping system. In: Proc. Int. Conf. Jets, Wakes Separated Flows, pp. 617–622.
Pickett, L.M., Ghandhi, J.B., 2001. Passive scalar measurements in a planar mixing layer by PLIF of acetone. Exp. Fluids 31, 309–318.

Pickett, L.M., Ghandhi, J.B., 2002. Passive scalar measurements in a planar shear layer with laminar and turbulent inlet conditions. Phys. Fluids 14, 985–998.

Tanaka, M., Murakami, S., Hibara, H., Sudo, K., 2005. Numerical simulation of the flow characteristics in T-junction with turbulence promoter. In: Proc. Int. Conf. Jets, Wakes Separated Flows, pp. 623–627.

Wu, H.L., Peng, X.F., Chen, T.K., 2003. Influence of sleeve tube on the flow and heat transfer behavior at a T-junction. Int. J. Heat Mass Trans. 46, 2637–2644.

Yuki, K., Tajima, Y., Toda, S., Hashidume, H., Muramatsu, T., 2004. Effect of curvature ratio on thermal mixing characteristics in a T-junction area which has a 90-degree bend in the upstream area. Trans. Jpn. Soc. Mech. Eng., B 70, 3142–3149 (in Japanese).